J Solid State Electrochem (2018) 22:1571–1580
DOI 10.1007/s10008-017-3700-6

ORIGINAL PAPER

Alachlor removal performance of $Ti/Ru_{0.3}Ti_{0.7}O_2$ anodes prepared from ionic liquid solution

Rodrigo de Mello[1] · Lucas H.E. Santos[1] · Marília M.S. Pupo[2] · Katlin I.B. Eguiluz[2] · Giancarlo R. Salazar-Banda[2] · Artur J. Motheo[1]

Received: 4 July 2017 / Revised: 10 July 2017 / Accepted: 12 July 2017 / Published online: 20 July 2017

Abstract Electrochemical processes have a considerable impact on the treatment of contaminated water and wastewater, since water reuse is becoming increasingly necessary. One of the most important variables in electrochemical degradation of organic substances is the electrode material. Several materials have been used successfully as anodes, highlighting those of boron-doped diamond and mixed metal oxide (MMO). The first one is characterized by the high generation of hydroxyl radicals while the second is well known for generating different oxidant species depending on the electrolyte solution composition. The present work aims to develop MMO anodes through thermal decomposition using 1-butylimidazolium hydrogen sulfate, an ionic liquid, as solvent in the precursor solution preparation. The ionic liquid prepared anodes characterization was performed by different techniques such as, scanning electron microscopy (SEM), X-ray diffraction and cyclic voltammetry, and their electrocatalytic performance was evaluated by the electrochemical degradation of alachlor. The commercial electrode presented larger internal area than the electrodes produced by the alternative method, but its efficiency was ca. 16% lower and its energy consumption was 16% higher than the laboratory-made electrode and calcined at 550 °C. Based on SEM results, this behavior can be attributed to the distribution of RuO_2 on the surface of the laboratory-made electrodes in comparison to the commercial one. Furthermore, the ionic liquid prepared electrodes showed an increase at least 8% in the voltammetric charge in the stability tests.

Keywords Mixed metal oxide · Ionic liquids · Organochlorine pollutants · Electrochemical degradation · Alachlor

Abbreviations
ILPE Ionic liquid prepared electrode

Introduction

The need to increase food production, seeking to supply the demand of a growing population, has as consequence the increase in the use of agricultural defensives, which intend to reduce the damage caused by plagues in many plantations [1]. Thus, with agriculture expansions and the increase in plague resistance to chemical products, improved considerably the introduction of persistent organic compounds in the environment, as well as the association of different compounds to increase their application [2]. The wide use of agricultural defensive has been associated with several environmental problems, of which water contamination is highlighted. Considering the high solubility of many substances, their entry in the hydric cycles is eased [3, 4] finding various routes, such as, direct disposal from industrial effluents and by lixiviation from plantations contaminated with pesticides, herbicides, fertilizers, etc.

Several agricultural defensives present organochloride in their compositions, since they present high chemical stability and are persistent in the environment [5, 6], which increases their lifetime for plague prevention. Alachlor (2-Chloro-N-(2, 6-diethylphenyl)-N-(methoxymethyl) acetamide) belongs to

✉ Artur J. Motheo
artur@iqsc.usp.br

[1] São Carlos Institute of Chemistry, University of São Paulo, Avenida Trabalhador São-carlense, 400, Parque Arnold Schmidt, São Carlos, SP 13566-590, Brazil

[2] Electrochemistry and Nanotechnology Laboratory, Research and Technology Institute/Processes Engineering Postgraduate-PEP, University Tiradentes, Avenida Murilo Dantas, 300, Farolândia, Aracaju, SE 49032-490, Brazil

chloroacetanilide family and is used as selective preemergent herbicide used to control the growth of annual grasses and broadleaf weeds in peanut, corn, and soy plantations [7]. In the USA, the use of alachlor is controlled [8], and in the European Community it was forbidden in 2006 because of its carcinogenic potential [9]. Bretveld et al. classified alachlor as endocrine disruptor because its mimicking action for the 17 β-estradiol hormone [10], and it is also capable to produce tumors in mammals [11].

Traditional biological processes are capable of removing alachlor after several treatment hours [12], while conventional physical-chemical processes do not present satisfactory performance to ensure an effective removal of this contaminant from effluents [13]. Considering the importance of removing alachlor from the environment, several degradation studies have been carried out using different processes, such as, photocatalysis [14], Fenton [15], and sonolysis [16], as well as combination of processes [17]. These studies, although highly efficient, present some inconvenient when considering their industrial application, such as, high cost. On the other hand, electrochemical process, presents advantages when compared with the remaining methods, like environmental compatibility, since they can lead to total mineralization (forming CO_2 and H_2O) of the organic compounds in the solution, besides being considered a clean technology, not requiring the use of chemical additives [18]. It is worth noting that electrochemical process can be used associated with other process as pre or post treatment, besides occupying a significantly smaller physical area when compared to conventional wastewater treatment plants [19].

In this context, the main challenge is the development of materials with high electrochemically active area, physical stability and with service lifetime adequate for industrial applications. In this sense, many materials have been successfully developed, for instance, boron-doped diamond (BDD) and mixed metal oxides (MMO), especially those denominated dimensionally stable anodes (DSA®). The BDD anodes are commonly known for producing hydroxyl radicals, favoring reactions in the solution bulk, while DSA® generate oxidant species from the anions present in the electrolytic solution, besides presenting electrochemical oxidation reactions on the surface of the anode [2].

The economic impact on the production of DSA® promoted their industrial application. Besides, the use of these anodes has been proven efficient in the oxidation of several organic compounds, such as, textile residues [20–23], formaldehyde-phenol solutions [24], esters dimethyl phthalate [25, 26], and atrazine herbicide [27, 28]. Research continue to explore MMO electrodes, conserving their low cost metallic substrate (Ti) over which the conductive metallic oxides are deposited through different techniques, among which thermal decomposition methods are highlighted, such as, polymeric precursors [29, 30] and sol-gel [31]. Although being known for some decades, many properties of these materials are not fully understood, such as their electrocatalytic nature and the relation between their electrochemical characteristics with their microstructure and physical-chemical properties, as well as the influence of synthesis method with their behavior [32].

Ionic liquid (IL) application in MMO electrodes synthesis has been focus of research only recently, where some of the physical properties of IL are explored [19, 33, 34]. The liquid state of these materials is reached at low temperatures because the low ionic interaction between the ions, since the cations are from organic compounds and generally larger than metallic cations. This feature enables the purification of IL by distillation in reduced pressure [35]. In this sense, the water solubility of the IL depends on both the anion and cation present, and in general will decrease with increasing organic character of the cation [36]. Among the advantages of IL use, the high viscosity and acidity of the solvent allow uniform distribution of metallic oxides on the electrode surface, with elimination of titanium oxides present on the surface of the substrate. Furthermore, IL presents low volatility, allowing combustion at higher temperatures (close to 500 °C), favoring the recovering of metal oxides on the substrate [33].

The aim of the present work is the development of electrodes composed by mixed metal oxides of 70% TiO_2 and 30% RuO_2 synthesized by thermal decomposition using the protic ionic liquid 1-butylimidazolium hydrogen sulfate solution for precursor solution preparation. The electroactivity of the electrodes was evaluated for eletrooxidation using alachlor as probe molecule, as a function of the calcination temperature and their performance settled by comparison with a commercial $Ti/Ru_{0.3}Ti_{0.7}O_2$ anode.

Experimental

Ionic liquid synthesis and characterization

1-butylimidazolium hydrogen sulfate ((HBIM)HSO_4) was synthesized in three stages: (i) production of sodium imidazole (NaIm) [37], (ii) production of functionalized N-imidazole [37], and (iii) reaction of N-imidazole functionalized with sulfuric acid (Fig. 1). The IL is obtained from the stoichiometric reaction of 1-butylimidazolium with sulfuric acid, adding the acid slowly and keeping the flask in an ice bath, once the temperature increase can lead to product degradation. The reagents used for synthesis were imidazole (Affymetrix, ultrapure), sodium hydroxide (Qhemis, 97% de purity), 1-bromobutane (Sigma-Aldrich, 99% de purity), and sulfuric acid (Qhemis, 95-98% de purity). The other solvents were used in a high purity grade. (HBIM)HSO_4 characterization was carried out with nuclear magnetic resonance of hydrogen (NMR–^{1}H) and of carbon (NMR–^{13}C). The spectra were obtained using Agilent 500/54 Premium Shielded equipment, from 16 scans,

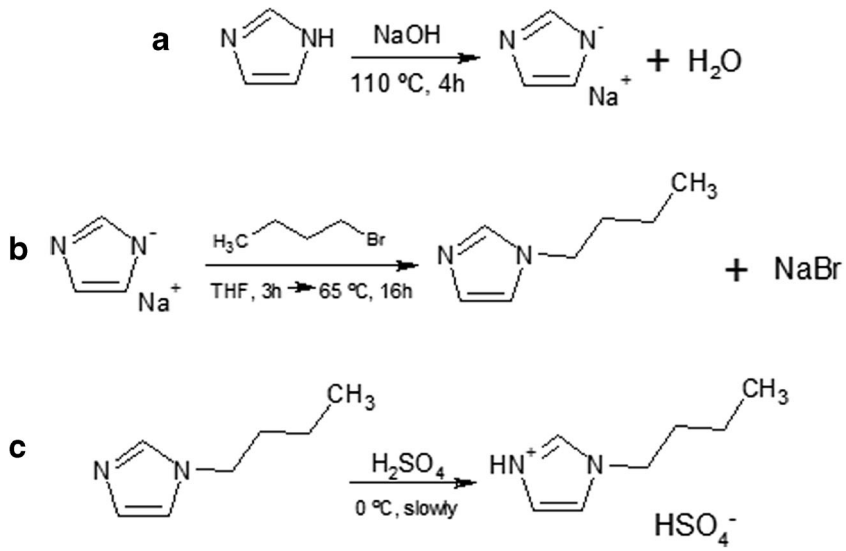

Fig. 1 Synthesis of $(HBIM)HSO_4$ from imidazole. **a** Production of sodium imidazolate. **b** Production of functionalized N-imidazole. **c** Reaction of N-functionalized with sulfuric acid

pulse of 3.85 μs (45°), spectral width of 8012 Hz (−2 to 14 ppm), acquisition time of 4.089 s, and relaxation of 1 s.

Preparation of MMO electrodes

The electrodes were prepared from titanium coupons with area ca. 1 cm^2, pretreated for impurities removal as described elsewhere [38]. The metallic precursor's solution was prepared by adapting a previous methodology [19]. According to this, 0.3 mol of ruthenium chloride (III) (Sigma-Aldrich, 99% purity) and 0.7 mol of titanium (IV) butoxide (Sigma-Aldrich, 97% purity) were dissolved in 1 mL of the IL $(HBIM)HSO_4$, in an ultrasound bath for 20 min at 50 °C. The solution was applied to the surface of the coupon by brushing and heated in an oven with a heating rate of 8 °C min^{-1} to a final temperature value of 500, 550, or 600 °C in which it was kept constant for 10 min. This procedure was repeated until a layer of ca. 1.2 mg cm^{-2} was reached, after which a final thermal treatment was carried out by 60 min.

Physical characterization

Morphological analysis of the electrode surfaces were carried out by scanning electronic microscopy (SEM) using a ZEISS LEO 440 (Cambridge, England) microscope with ×5000 magnification using an OXFORD (model 7060) detector. The composition of the surface of the films was determined by energy dispersive spectroscopy (EDS), and the distribution of metals on surface was verified by mapping. The crystalline structure was analyzed by X-ray diffractometry using a Bruker (model D8 Advance) diffractometer with a Cu source and detector sensible to positioning. The detection conditions were $2\theta = 5–80°$, with a 0.025° and irradiation time of 0.5 s by step.

Electrochemical characterization

Cyclic voltammetric experiments were done in a single compartment glass cell with (i) MMO as working electrode, (ii) Pt plate as counter-electrode, (iii) reversible hydrogen electrode (RHE) as reference, at scan rates ranging from 2.5 to 300 mV s^{-1}. The analyses were performed in Na_2SO_4 0.033 mol L^{-1} supporting electrolyte solution using a PGSTAT128N potentiostat/galvanostat (Metrohm Autolab B.V., The Netherlands), controlled by the software Nova 2.0.

Alachlor electrooxidation

The electrooxidation experiments were carried out in 100 mL of Na_2SO_4 0.033 mol L^{-1} solution containing 100 mg L^{-1} of alachlor at pH = 3.0 and 25 °C. It was used a glass cell with a single compartment containing a MMO anode and a titanium sheet cathode. The applied current density was 30 mA cm^{-2} during 2 h, and the potential difference between the electrodes was monitored to evaluate the energetic efficiency. The concentration decay of alachlor was determined using a Shimadzu LC–10ADVP liquid chromatograph, with UV detector (model 10 AVP), connected in series and a reverse phase C18 column (Ascentis; 15 cm × 4.6 mm, 3 μm). The eluent used in the mobile phase, in isocratic mode, was acetonitrile and water, 70:30 (in volume ratio), operating with flow of 1.2 mL min^{-1}, with detection wavelength at 196 nm.

Results

$(HBIM)HSO_4$ characterization

By the NMR–^{1}H (Fig. 2a) and NMR–^{13}C (Fig. 2b) spectra obtained for the IL synthesized, it is possible to observe

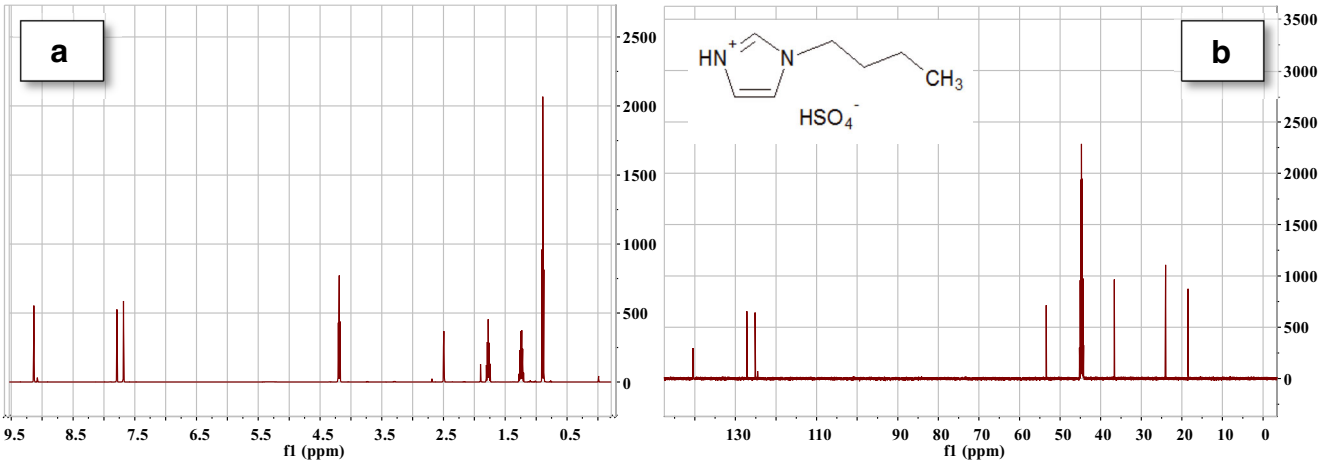

Fig. 2 NMR analysis of the ionic liquid (HBIM)HSO_4. **a** NMR–^{1}H spectra (499.85 MHz). **b** NMR–^{13}C spectra (125.7 MHz); DMSO-d_6 solvent, T = 25 °C

chemical shifts associated with imidazole at 7.6–7.8 and 9.0 ppm in the NMR–^{1}H spectra, as well as 120.0–123.0 and 136.0 ppm in the NMR–^{13}C spectra. The chemical shifts observed in 0.9, 1.2, 1.8, and 4.2 ppm in Fig. 2a (NMR–^{1}H) and 13.2, 19.3, 32.0, and 48.5 ppm in Fig. 2b (NMR–^{13}C) are associated to the carbon chain connected to the imidazole ring. The solvent used (dimethyl sulfoxide-d_6, DMSO-d_6) is responsible for the chemical shifts located in 2.5 and 40.0 ppm of the NMR–^{1}H and NMR–^{13}C spectra, respectively [39]. The analysis of the results obtained allowed concluding that (HBIM)HSO_4 was successfully synthesized, and that there was no significant rearrangement in the carbon chain, as for example, for the tert-butyl or any other ramification.

Physical characterization of MMO electrodes

Figure 3 shows the images obtained by SEM of the electrodes produced using (HBIM)HSO_4 calcined at 500 °C (Fig. 3a), 550 °C (Fig. 3b), and 600 °C (Fig. 3c) and of the commercial electrode (Fig. 3d) in which the mud-cracked aspect is seen, similar to other metal oxide films deposited by thermal decomposition method [19, 40]. In the films produced using (HBIM)HSO_4 in the precursor solution, a more compact appearance was seen, with the formation of grains on the surface and cracks not well defined, as compared to the commercial electrode. The increase in calcination temperature contributes even more

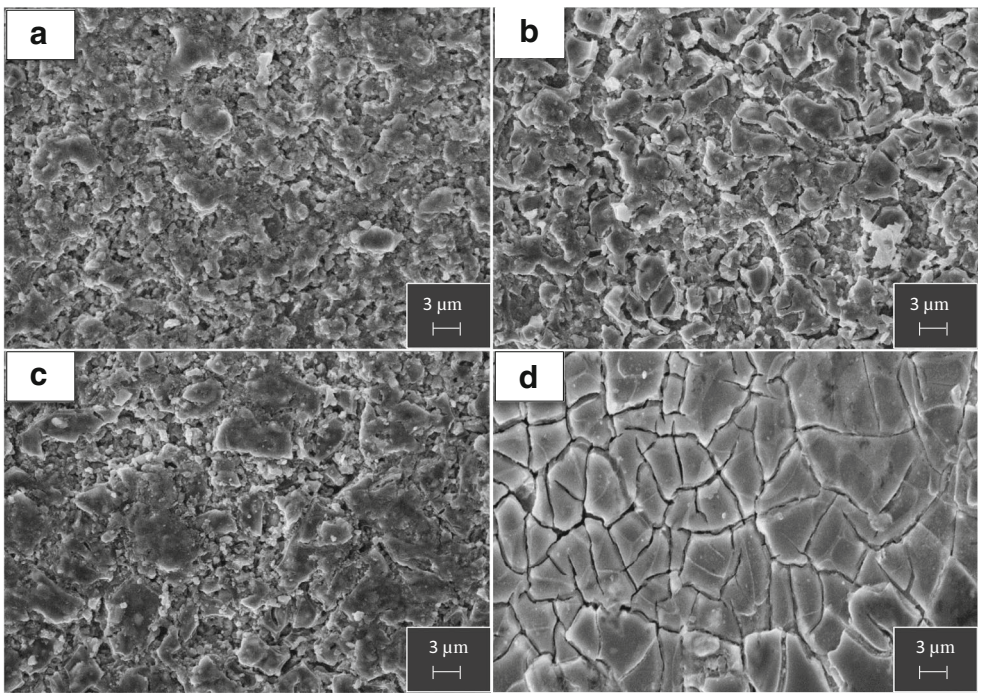

Fig. 3 SEM images of the electrodes surfaces with nominal composition of Ti/$Ru_{0.3}Ti_{0.7}O_2$ obtained using (HBIM)HSO_4 during precursor solution preparation and calcined at **a** 550, **b** 550, and **c** 600 °C, as well as **d** commercial electrode. Magnification ×5.000

Table 1 Nominal and real composition of the laboratory-made using $(HBIM)HSO_4$ and commercial electrodes

	Nominal Composition (% Ru)	Real Composition (% Ru)
Commercial	30	24
500 °C	30	44
550 °C	30	40
600 °C	30	32

for these features, besides promoting certain inhomogeneity on the structure. As seen in previous studies, because its high combustion temperature (~450 °C [41]), the materials prepared using $(HBIM)HSO_4$ in the precursor solution preparation, tend to present more compact structures with less representative cracks, which can be attributed to the protective effect that IL have during the dilatation and contraction of recovering layers and the metallic support [34].

The real composition of the surface of the films is shown in Table 1. The increased calcination temperature increased the amount of Ru deposited. This influences the efficiency of the electrodes during the electrooxidation process, since this metal is responsible for the catalytic activity of the electrodes [40]. Besides that, the mapping of the surface (Fig. 4) reveals a homogeneous distribution of Ru on electrodes prepared using $(HBIM)HSO_4$ on precursor solution, while on commercial electrode presents this metal more concentrate on the boundary of the islands.

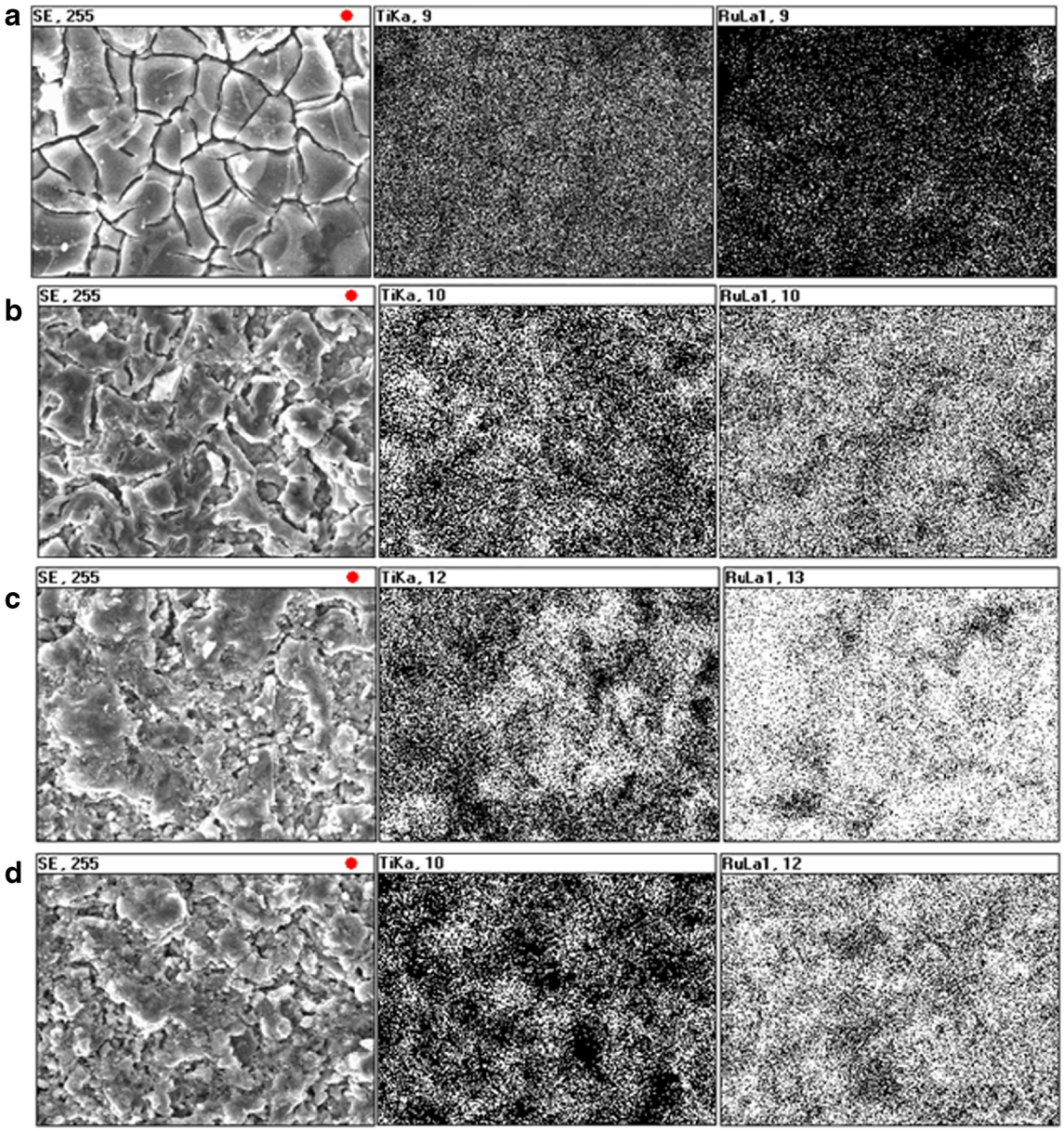

Fig. 4 Mapping of surface of the laboratory-made electrodes calcined at **a** 500, **b** 550, and **c** 600 °C and **d** commercial electrodes

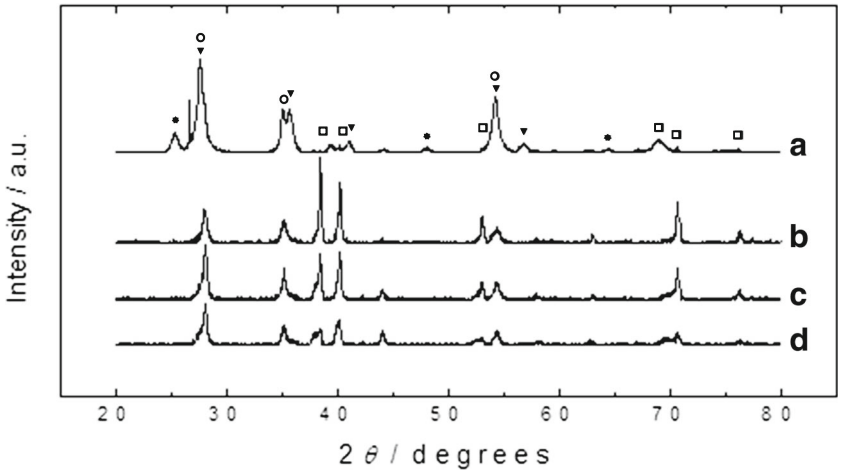

Fig. 5 X-ray diffractograms of the electrodes with nominal composition $Ti/Ru_{0.3}Ti_{0.7}O_2$. Commercial electrode (**a**) and the electrodes obtained using $(HBIM)HSO_4$ during precursor solution preparation calcined at 500 (**b**), 550 (**c**), and 600 °C (**d**). (✷) TiO_2 anatase, (▼) TiO_2 rutile, (○) RuO_2 rutile, (□) Ti

XRD analysis shown in Fig. 5 locate the peaks, and the intensities of the diffractograms compared with the standards of the Joint Committee on Powder Diffractions Standards (JCPDS). Anatase phase of TiO_2 (JCPDS 78-2486), which is related to the crystalline phase that presents photoactivity superior to rutile phase was found only in the commercial electrode. It is worth noting that the thermal treatment temperature influences the crystalline structure of the films as described by Guillard et al. [42], who analyzed the effect of calcination temperature in the photocatalytic activity of TiO_2 films produced by sol-gel method. In temperatures lower than 200 °C, the rutile phase was not verified. These results are in accordance with the findings of Lin et al. [43]. For the electrodes produced in the present work, the rutile phase was observed (JCPDS 21-1276), as seen in literature [44], where producing Ti/TiO_2RuO_2 by polymeric precursor method calcined at 400 °C presented only rutile phase of TiO_2. Besides, the ruthenium oxide phase obtained during thermal decomposition was rutile as well (JCPDS 40-1290). The overlapping of metallic oxide peaks is concerning to the response obtained from the reflection of similar planes. However, it is possible to observe peaks corresponding to titanium substrate (JCPDS 44-1294). These peaks are more intense in electrodes produced in the present work, which indicates that the films are thinner in comparison to the commercial electrode, and therefore, present higher penetration of X-rays, reaching the substrate more intensely [19].

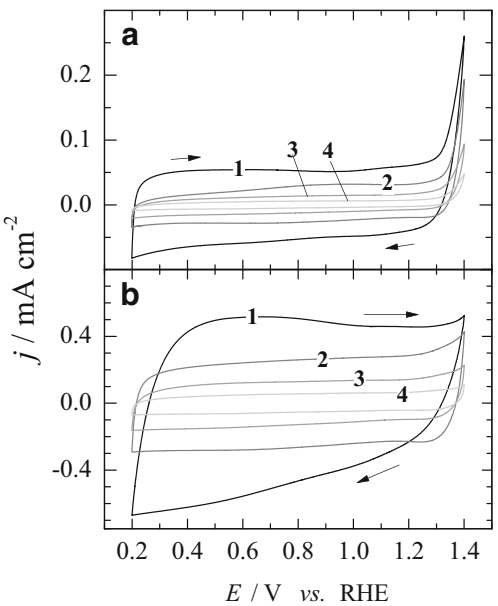

Fig. 6 Cyclic voltammograms of nominal composition $Ti/Ru_{0.3}Ti_{0.7}O_2$ electrodes in 0.033 mol L^{-1} Na_2SO_4. Commercial electrode (*1*) and the electrodes produced using $(HBIM)HSO_4$ as solvent with calcination temperatures of 500 (*2*), 550 (*3*), and 600 °C (*4*). *Scan rate* (**a**) 5 mV s^{-1} and **b** 50 mV s^{-1}

Electrochemical characterization of the MMO electrodes

In Fig. 6a, b, the third cycle of the voltammograms obtained at 5 and 50 mV s^{-1}, respectively, are presented for the prepared anodes prepared using $(HBIM)HSO_4$ and the commercial one. It is possible to observe that thermal treatment has direct relation with the electrochemical active area of the electrode, where the increase in calcination temperature, promotes a reduction in electrochemical active area of the electrode. As reported previously by Ouattara et al. [45], the increase in calcination temperature promotes the growth of the TiO_2 insulating layer between the substrate and the deposited film, reducing its conductivity. Another factor that can influence this effect is the reduction in active sites caused by the increase in grain size, agglomeration, and increase in crystallinity when high temperatures are used [29]. Considering that the commercial electrode presents a higher voltammetric area, it also presents an electrochemically active area superior to those electrodes produced in the present work.

From the analysis of anodic charge variation with scan rate (Fig. 7), it is possible to verify that anodic charge of the

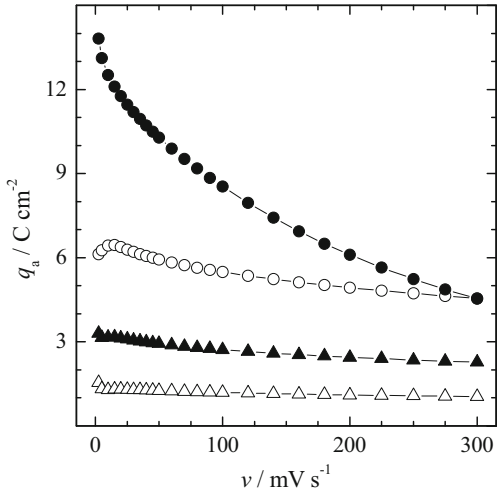

Fig. 7 Anodic charge variation with scan rate for nominal composition $Ti/Ru_{0.3}Ti_{0.7}O_2$ electrodes. (●) commercial and ionic liquid prepared anode using $(HBIM)HSO_4$ calcined at (○)500, (▲)550, and (Δ) 600 °C

electrodes produced in the present work decay with the increase in calcination temperature. The anodic charge considering the lower scan rate represent a response of electrodes internal sites and external sites [46]. The commercial electrode presents the highest charge values at low scan rates and a considerable decrease with the increase of the sweep-rate. It is possible to conclude that it presents higher internal area than the electrodes produced by the thermal decomposition method using $(HBIM)HSO_4$ for precursor solution, and that the internal sites of commercial electrode has a low interaction with the solution when high scan rates are used [46]. The electrode produced using $(HBIM)HSO_4$ and calcined at 500 °C presents a high anodic charge at high scan rates, similar to that obtained for the commercial electrode, which indicates that these electrodes present similar electrochemically active area in these scan rates. Therefore, it is expected that these electrodes present similar behavior in higher scan rates.

The determination of total differential and external capacitance allows to calculate the morphology factor (φ_{mor}), which is the measure of contribution of internal sites of the electrodes to the total differential capacitance [47]:

$$\varphi_{mor} = \frac{C_{d,i}}{C_{d,t}} \quad (1)$$

Where $C_{d,i}$ e $C_{d,t}$ correspond to the internal and total differential capacitance, respectively, representing therefore corresponding superficial areas. The values of φ_{mor} can vary from 0 to 1, where values closer to 1 indicate a high internal area of the electrode [47]. The values of $C_{d,i}$, $C_{d,t}$, $C_{d,e} = C_{d,t} - C_{d,i}$ and φ_{mor} were determined for the electrodes produced by the method using $(HBIM)HSO_4$ for the synthesis of the precursor solution and for the commercial electrode using methodology presented by Da Silva et al. [47] and are presented in Table 2.

Table 2 Total differential capacitance ($C_{d,t}$), external differential capacitance ($C_{d,e}$), internal differential capacitance ($C_{d,i}$) and morphology factor (φ_{mor}) of commercial electrode and those prepared from ionic liquids with composition $Ti/Ru_{0.3}Ti_{0.7}O_2$

	$C_{d,t}$(mF cm^{-2})	$C_{d,e}$(mF cm^{-2})	$C_{d,i}$(mF cm^{-2})	φ_{mor}
Commercial	9.09	0.54	8.55	0.94
500 °C	3.44	0.99	2.45	0.71
550 °C	2.88	0.98	1.90	0.66
600 °C	0.61	0.46	0.15	0.25

As can be seen, commercial electrode presents a higher $C_{d,t}$, which means that it presents a higher superficial total area when compared to the electrodes synthetized using $(HBIM)HSO_4$. As the commercial electrode presents a very low $C_{d,e}$, it is possible to conclude that the majority of active sites in these electrodes are in the internal area. The φ_{mor} of the electrodes produced by the method proposed reduce with the increase of calcination temperature, which indicates a reduction in internal area of these electrodes, as expected considering the anodic charge values as well as from the cyclic voltammetric profiles. Besides, these results confirm the predominance of internal area in the commercial electrode.

The stability of the electrodes was analyzed by cyclic voltammetry at 50 mV s^{-1}, in which the 2nd and 1,000th cycles are represented in Fig. 8. In case of the electrodes produced in the present work, it is possible to note an increase in electrochemically active area on the last cycle, while the commercial electrode presented a reduction in 6%. This indicates that the electrodes produced using $(HBIM)HSO_4$ in the precursor solution become more active after the tests. Besides, the electrodes

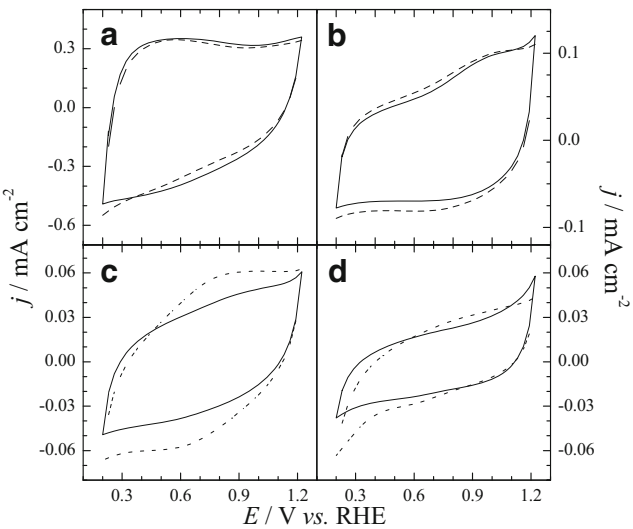

Fig. 8 Cyclic voltammograms of the commercial electrode (**a**) and the the ionic liquid prepared electrodes using $(HBIM)HSO_4$ calcined at **b** 500, **c** 550, and **d** 600 °C. 2nd cycle (*continuous line*) and 1,000th cycle (*dotted line*). Electrolytic solution 0.033 mol L^{-1} Na_2SO_4. *Scan rate* 50 mV s^{-1}

Table 3 Anodic charge (q_a), cathodic charge (q_c), and ratio of charges to 2nd (initial) and 1,000th (final) cycle at 50 mV s^{-1} in 0.033 mol L^{-1} Na_2SO_4 solution containing 100 mg L^{-1} to the electrodes with composition $Ti/Ru_{0.3}Ti_{0.7}O_2$

	Initial			Final		
	q_a	q_c	$\frac{q_a}{q_c}$	q_a	q_c	$\frac{q_a}{q_c}$
Commercial	5.95	6.09	0.98	5.64	5.66	1.00
500 °C	1.21	1.15	1.05	1.29	1.33	0.97
550 °C	0.56	0.63	0.89	0.80	0.79	1.02
600 °C	0.38	0.36	1.06	0.39	0.40	0.98

presented a higher electrochemical reversibility for the final cycles, as can be seen in Table 3.

Alachlor electrooxidation

The electrodes produced by thermal decomposition using $(HBIM)HSO_4$ during the preparation of precursor solution were used for electrolysis of alachlor herbicide in order to analyze their catalytic activity. The electrolyses were carried out in 0.033 mol L^{-1} Na_2SO_4 with 100 mg L^{-1} of alachlor, in which the pH was adjusted to 3.0.

According to Pipi et al. [13], the kinetic behavior of the electrooxidation of alachlor is of pseudo-first order. The results obtained in this work adjust to this kinetic profile, as presented in Fig. 9. The values of rate constant, presented in Table 4, can be obtained from the slope of the $\ln(C_t/C_0)$ vs. t curves, according to Eq. 2.

$$\ln\left(\frac{C_t}{C_0}\right) = -kt \tag{2}$$

where c_0 and c_t are the initial and final concentration, respectively, k is the rate constant and t the reaction time.

From analysis of Table 4, it is possible to note that the electrodes produced in this work presented a higher efficiency when compared to the commercial electrode, since they present a decay in the concentration of alachlor around 15% higher when compared with commercial electrode. Jara et al. [33] synthesized MMO electrodes by different thermal decomposition methods and observed that the electrodes synthesized by the IL method were more efficient towards the oxidation of an organic pollutant. They concluded that the IL method provides electrodes with a relatively higher superficial area in comparison to the other methods. In our work, the differential capacitance studies indicate that the commercial electrode has a higher superficial area than the synthesized electrodes. Therefore, the higher efficiency of the synthesized electrodes can be related to other aspects, such as the distribution of the active sites on the surface of the electrodes. As showed by mapping (Fig. 4), the Ru is covering the entire surface of the ionic liquid prepared electrodes, providing a greater electrochemical active area than the commercial one. Santos et al. [19] showed that the IL method is more efficient to recover the substrate than other methods on deposition of RuO_2, depending on the thermal decomposition method used, and related this to the availability of the active sites. Another factor that contributed to the superior efficiency of the electrodes produced in the laboratory is that alachlor is a relatively large molecule. Since the commercial electrode has a greater number of internal active sites (inside the cracks), the access of the contaminant molecules becomes more difficult, reducing their removal during the electrooxidation process. In addition, the applied current density generates a large amount of gases at the surface of the electrode, further impeding the access of the molecule to the internal active sites.

Pipi et al. [13] studied the removal of alachlor by combining several advanced oxidation processes (AOP) and obtained complete mineralization of the herbicide by the photoelectron-Fenton process after 360 min using a BDD as anode. In this study, the pseudo-first order rate constant for the removal of alachlor by H_2O_2-assisted electrooxidation process was 1.38 10^{-4} s^{-1} that equals to 8.28 10^{-3} min^{-1}. This value is comparable to the rate constants determined in our work for the MMO laboratory-made electrodes (Table 4), which represents

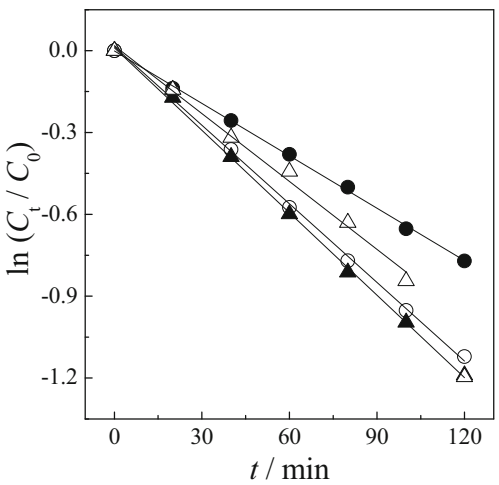

Fig. 9 Kinetic analysis for the electrooxidation of 100 mg L^{-1} alachlor in 0.033 mol L^{-1} Na_2SO_4 at 30 mA cm^{-2} considering a pseudo-first order reaction. Commercial electrode (●) and electrodes produced using $(HBIM)HSO_4$ calcined at (○)500, (▲)550, and (Δ) 600 °C

Table 4 Alachlor removal, pseudo-first order rate constant and energy consumption (EC_E) values obtained for electrochemical degradation of 100 mg L^{-1} of alachlor in 0.033 mol L^{-1} Na_2SO_4 solution by the application of 30 mA cm^{-2} using the electrodes with composition Ti/$Ru_{0.3}Ti_{0.7}O_2$

	% Removal	$k/10^{-3}$ min^{-1}	EC_E/kW h m^{-3}
Commercial	53.8	6.4	3.55
500 °C	67.4	9.6	3.14
550 °C	69.6	10.0	2.99
600 °C	65.8	8.3	3.26

a considerable outcome since H_2O_2-assistance was not used in our experiments.

Other processes were applied for the degradation of alachlor, for instance, Fenton-assisted heterogeneous photocatalysis by TiO_2 [48], sonochemical process [49], photoelectrooxidation by TiO_2 nanotubes [50] and Fenton-assisted sonochemical process [7]. It is evident from the publications that the combination of processes results in higher removal efficiencies: complete alachlor removal can be achieved within 120 min or less. In our study, alachlor removal efficiency of ca. 70% was achieved after 120 min by unassisted electrooxidation using the MMO electrode calcined at 550 °C as anode. This is also a considerable outcome because the operational costs should be lower for simple electrochemical process than for combined processes.

Conclusion

Thermal decomposition using (HBIM)HSO_4 as solvent in the preparation of precursor solution for the production of MMO electrodes is a viable and economic alternative, since it requires lower production time, due to the physical-chemical properties of IL, which positively affects the metal oxides formation. Besides, the electrodes produced have performance slightly superior to the commercial electrode for electrooxidation of alachlor, with degradation efficiencies up to 16% higher than that presented by the commercial one. This is can be related to the fact that the commercial electrode presents a greater amount of internal active sites, which are accessed through the cracks in its surface. Since alachlor is a large molecule, its access to such sites is impaired. Moreover, the use of (HBIM)HSO_4 provided a better distribution of catalyst metal on surface of the electrode, improving its catalytic activity.

Acknowledgements The authors thank the financial support from São Paulo Research Foundation (FAPESP), Sergipe State Research and Technological Innovation Foundation (FAPITEC/SE), the Coordination for the Improvement of Higher Education Personnel (CAPES), and the National Council for Scientific and Technological Development (CNPq: 130849/2016-2, 304419/2015-0, 140669/2014-0 and 310282/2013-6).

References

1. Primel EG, Zanella R, Kurz MHS, Gonçalves FF, Machado SO, Marchezan E (2005) Pollution of water by herbicides used in the irrigated rice cultivation in the central area of Rio Grande do Sul state, Brazil: theoretical prediction and monitoring. Quím Nova 28(4):605–609
2. Martínez-Huitle CA, Rodrigo MA, Sirés I, Scialdone O (2015) Single and Coupled Electrochemical Processes and Reactors for the Abatement of Organic Water Pollutants: A Critical Review. Chem Rev 115(24):13362–13407
3. Oller I, Malato S, Sanchez-Perez JA (2011) Combination of advanced oxidation process and biological treatments for wastewater decontamination. A review. Sci Total Environ 409(20):4141–4166
4. Konstantinou IK, Hela DG, Albanis TA (2006) The status of pesticide pollution in surface waters (rivers and lakes) of Greece. Part I. Review on occurrence and levels. Environ Pollut 141(3):555–570
5. Verhaert V, Newmark N, D'Hollander W, Covaci A, Vlok W, Wepener V, Addo-Bediako A, Jooste A, Teuchies J, Blust R, Bervoets L (2017) Persistent organic pollutants in the Olifants River Basin, South Africa: Bioaccumulation and trophic transfer through a subtropical aquatic food web. Sci Total Environ 586: 792–806
6. Chopra AK, Sharma MK, Chamoli S (2011) Bioaccumulation of organochlorine pesticides in aquatic system—an overview. Environ Monit Assess 173:905–916
7. Wang C, Liu C (2014) Decontamination of alachlor herbicide wastewater by a continuous dosing mode ultrasound/Fe2+/H2O2 process. J Environ Sci 26(6):1332–1339
8. Human Health - water ingestion only Fact Sheet for Alachlor: (Human Health Carcinogen - water ingestion only), New York State Department of Environmental Conservation (1998) US EPA https://www.epa.gov/gliclearinghouse/human-health-water-ingestion-only-fact-sheet-alachlor-human-health-carcinogen-water. Accessed 28 Apr 2017
9. What substances are banned and authorised in the EU market? http://www.pan-europe.info/old/Archive/About%20pesticides/Banned%20and%20authorised.htm. Accessed 15 May 2017
10. Bretveld RW, Thomas CMG, Scheepers PTJ, Zielhuis GA, Roeleveld N (2006) Pesticide exposure: the hormonal function of the female reproductive system disrupted?. Reprod Biol Endocrinol 4:30–43
11. Crawford G, Hurrel P, Paroschy K, Pereira C (2017) Pharmaceuticals and other endocrine disrupting compounds in natural water systems. Muskoka Watershed Council, Bracebridge
12. Szewczyk R, Sobon A, Slaba M, Dlugonski J (2015) Mechanism study of alachlor biodegradation by Paecilomyces marquandii with proteomic and metabolomic methods. J Hazard Mater 291:52–64
13. Pipi ARF, Andrade AR, Brillas E, Sirés I (2014) Total removal of alachlor from water by electrochemical processes. Sep Purif Technol 132:674–683
14. Luna MDG, Rivera KKP, Suwannaruang T, Wantala K (2016) Alachlor photocatalytic degradation over uncalcined Fe-TiO2 loaded on granular activated carbon under UV and visible light irradiation. Desalin Water Treat 57:6712–6722
15. Bolobajev J, Trapido M, Goi A (2015) Improvement in iron activation ability of alachlor Fenton-like oxidation by ascorbic acid. Chem Eng J 281:566–574
16. Kidak R, Dogan S (2015) Degradation of trace concentrations of alachlor by medium frequency ultrasound. Chem Eng Process 89: 19–27
17. Wang C, Liu Z (2015) Degradation of alachlor using an enhanced sono-Fenton process with efficient Fenton's reagent dosages. J Environ Sci Health B 50(7):504–513

18. Juttner K, Galla U, Schmieder H (2000) Electrochemical approaches to environmental problems in the process industry. Electrochim Acta 45:2575–2594
19. Santos TES, Silva RS, Jara CC, Eguiluz KIB, Salazar-Banda GR (2014) The influence of the syntesis method of Ti/RuO_2 electrodes on their stability and catalytic activity for electrochemical oxidation of the pesticide carbaryl. Mater Chem Phys 148(1–2):39–47
20. Malpass GRP, Miwa DW, Mortari DA, Machado SAS, Motheo AJ (2007) Decolorisation of real textile waste using electrochemical techniques: effect of the chloride concentration. Water Res 41(13): 2969–2977
21. Malpass GRP, Miwa DW, Machado SAS, Motheo AJ (2008) Decolourisation of real textile waste using electrochemical techniques: Effect of electrode composition. J Hazard Mater 156(1–3):170–177
22. Rajkumar D, Kim JG (2006) Oxidation of various reactive dyes with in situ electro-generated active chlorine for textile dyeing industry wastewater treatment. J Hazard Mater 136(2):203–212
23. Alves PA, Malpass GRP, Johansen HD, Azevedo EB, Gomes LM, Vilela WF, Motheo AJ (2010) Photoassisted electrochemical degradation of real textile wastewater. Water Sci Technol 61(2):491–498
24. Fornazari ALT, Malpass GRP, Miwa DW, Motheo AJ (2012) Application of electrochemical degradation of wastewater composed of mixtures of phenol-formaldehyde. Water Air Soil Poll 223(8):4895–4904
25. Souza FL, Aquino JM, Miwa DW, Rodrigo MA, Motheo AJ (2014) Electrochemical degradation of dimethyl phthalate ester on a DSA® electrode. J Braz Chem Soc 25(3):492–501
26. Souza FL, Aquino JM, Miwa DW, Rodrigo MA, Motheo AJ (2014) Photo-assisted electrochemical degradation of the dimethyl phthalate ester on DSA® electrode. J Environ Chem Eng 2(2):811–818
27. Malpass GRP, Miwa DW, Gomes L, Azevedo EB, Vilela WFD, Fukunaga MT, Guimaraes JR, Bertazzoli R, Machado SAS, Motheo AJ (2010) Photo-assisted electrochemical degradation of the comercial herbicide atrazine. Water Sci Technol 62(12):2729–2736
28. Malpass GRP, Miwa DW, Santos RL, Vieira EM, Motheo AJ (2012) Unexpected toxicity decrease during photoelectrochemical degradation of atrazine with NaCl. Environ Chem Lett 10(2):177–182
29. Terezo AJ, Pereira EC (1999) Preparation and characterization of Ti/RuO2–Nb2O5 electrodes obtained by polymeric precursor method. Electrochim Acta 44(25):4507–4513
30. Pechini MP (1963) Method of preparing lead and alkaline earth titanates and niobates and coating method using the same to form a capacitor. US Patent US3330697A
31. Kakihana M (1996) Invited Review "Sol-gel" preparation of high temperature superconducting oxides. J Sol-gel Sci Techn 6(1):7–55
32. Alves VA, Silva LA, Boodts JFC (2000) Análise por difração de raios X de filmes de óxidos cerâmicos compostos por IrO2/TiO2/CeO2. Quím Nova 23(5):608–613
33. Jara CC, Salazar-Banda GR, Arratia RS, Campino JS, Aguilera MI (2011) Improving the stability of Sb doped Sn oxides electrode thermally synthesized by using an acid ionic liquid as solvent. Chem Eng J 171(3):1253–1262
34. Santos TES, Silva RS, Eguiluz KIB, Salazar-Banda GR (2015) Development of Ti/(RuO2)0.8 (MO2)0.2 (M=Ce, Sn or Ir) anodes for atrazine electro-oxidation. Influence of the synthesis method. Mater Lett 146:4–8
35. Earle MJ, Esperança JMSS, Gilea MA, Lopes JNC, Rebelo LPN, Magee JW, Seddon KR, Widegren JA (2006) The distillation and volatility of ionic liquids. Nature 439:831–834
36. Wasserscheid P, Welton T (2008) Ionic liquids in synthesis. Wiley-VCH, Weinheim
37. Bara JE (2011) Versatile and scalable method for producing N-functionalized imidazoles. Ind Eng Chem Res 50(24):13614–13619
38. Pupo MMS, Costa LS, Figueiredo AC, Silva RS, Cunha FGC, Eguiluz KIB, Salazar-Banda GR (2013) Photoelectrocatalytic Degradation of Indanthrene Blue Dye using Ti/Ru-Based Electrodes Prepared by a Modified Pechini Method. J Braz Chem Soc 24(3):459–472
39. Gottlieb HE, Kotlyar V, Nudelman A (1997) NMR Chemical Shifts of Common Laboratory Solvents as Trace Impurities. J Org Chem 62:7512–7515
40. Forti JC, Olivi P, Andrade AR (2001) Characterization of DSA®-type coatings with nominal composition Ti/Ru0,3Ti(0,7-x)SnxO2 prepared via a polymeric precursor. Electrochim Acta 47(6):913–920
41. Meindersma GW, Maase M, de Haan AB (2012) In: Elvers B (ed-in-chief) Ullmann's Encyclopedia of Industrial Chemistry, v. 19. Wiley-VCH, Weinheim
42. Guillard C, Beaugiraud B, Dutriez C, Herrmann JM, Jaffrezic H, Jaffrezic-Renault N, Lacroix M (2002) Physicochemical properties and photocatalytic activities of TiO2-films prepared by sol–gel methods. Appl Cat B 39(4):331–342
43. Lin CP, Chen H, Nakaruk A, Koshy P, Sorrell CC (2013) Effect of Annealing Temperature on the Photocatalytic Activity of TiO2 Thin Films. Energy Proced 34:627–636
44. Gonzalez IL, Moreira JAB, Andrade AR, Ribeiro J (2016) Estudo da Reação de Desprendimento de Oxigênio em Eletrodos do Tipo Ta/RuO2-Ta2O5-TiO2. Rev Virtual Quím 8(5):1347–1365
45. Ouattara L, Diaco T, Duo I, Panizza M, Foti G, Comninellis C (2003) Dimensionally Stable Anode-Type Anode Based on Conductive p-Silicon Substrate. J Electrochem Soc 150(2):D41–D45
46. Kodintsev IM, Trasatti S, Rubel M, Wieckowski A, Kaufher N (1992) X-ray photoelectron spectroscopy and electrochemical surface characterization of IrO2 + RuO2 electrodes. Langmuir 8(1): 283–290
47. Da Silva LM, Faria LA, Boodts JFC (2001) Determination of the morphology factor of oxide layers. Electrochim Acta 47(3):395–403
48. Maldonado MI, Passarinho PC, Oller I, Gernjak W, Fernández P, Blanco J, Malato S (2007) Photocatalytic degradation of EU priority substances: A comparison between TiO2 and Fenton plus photo-Fenton in a solar pilot plant. J Photoch Photobio A 185(2–3):354–363
49. Torres RA, Mosteo R, Pétrier C, Pulgarin C (2009) Experimental design approach to the optimization of ultrasonic degradation of alachlor and enhancement of treated water biodegradability. Ultrason Sonochem 16(3):425–430
50. Xin Y, Liu H, Han L, Zhou Y (2011) Comparative study of photocatalytic and photoelectrocatalytic properties of alachlor using different morphology TiO2/Ti photoelectrodes. J Hazard Mater 192(3):1812–1818